Title

Automated Beta Zone Parapapillary Area Measurement to Differentiate Between Healthy and Glaucoma Eyes

Authors

Manalastas, Patricia Isabel C
Belghith, Akram
Weinreb, Robert N
et al.

Publication Date

2018-07-01

DOI

10.1016/j.ajo.2018.04.021

Peer reviewed

HHS Public Access

Author manuscript

Am J Ophthalmol. Author manuscript; available in PMC 2019 July 01.

Published in final edited form as:

Am J Ophthalmol. 2018 July ; 191: 140–148. doi:10.1016/j.ajo.2018.04.021.

Automated Beta Zone Parapapillary Area Measurement to Differentiate Between Healthy and Glaucoma Eyes

Patricia Isabel C. Manalastas[1], **Akram Belghith**[1], **Robert N. Weinreb**[1], **Jost B. Jonas**[2], **Min Hee Suh**[1,3], **Adeleh Yarmohammadi**[1], **Felipe A. Medeiros**[1], **Christopher A. Girkin**[4], **Jeffrey M. Liebmann**[5], and **Linda M. Zangwill**[1]

[1]Hamilton Glaucoma Center, Shiley Eye Institute and Department of Ophthalmology, University of California, San Diego, La Jolla, CA, United States

[2]Department of Ophthalmology, Medical Faculty Mannheim, Ruprecht-Karls-University of Heidelberg, Mannheim, Germany

[3]Ophthalmology, Haeundae Paik Hospital, Inje University, Busan, South Korea

[4]Department of Ophthalmology, School of Medicine, University of Alabama, Birmingham, United States

[5]Bernard and Shirlee Brown Glaucoma Research Laboratory, Edward S. Harkness Eye Institute, Department of Ophthalmology, Columbia University Medical Center, New York, NY

Abstract

Purpose: To evaluate whether automated assessment of beta-zone parapapillary atrophy (ßPPA) area can differentiate between glaucomatous and healthy eyes of varying axial lengths (AL).

Design: Cross-sectional study.

Methods: ßPPA was automatically identified in glaucoma and healthy eyes with enhanced depth imaging optical coherence tomography (OCT) optic nerve head (ONH) radial B-scans. Associations with AL and the presence of glaucoma were assessed. Manually-delineated ßPPA on individual OCT ONH B-scans of 35 eyes from the Diagnostic Innovations in Glaucoma Study served to validate the automated method.

Results: One hundred fifty-three glaucoma eyes (mean ± SD) (visual field mean deviation: −5.0 ± 6.4 dB and mean axial length, 25.1 ± 1.1 mm) and 73 healthy eyes (visual field mean deviation, 0.1 ± 1.4 dB; and mean axial length 24.1 ± 1.1 mm) were included. In multivariable analysis, larger ßPPA area was significantly associated with a diagnosis of glaucoma after controlling for age, central corneal thickness, and axial length. Moreover, in multivariable analysis, the odds of having glaucoma were doubled for each 0.2 mm^2 larger ßPPA area. The age- and AL-adjusted area under the receiver operating characteristic curve (95% CI) of ßPPA area for differentiating

Corresponding Author: Linda M. Zangwill, PhD, Hamilton Glaucoma Center, Shiley Eye Institute, University of California, San Diego, 9415 Campus Point Drive, La Jolla, CA 92037, Phone number: 858-534-7686, lzangwill@ucsd.edu.

between glaucoma and healthy eyes was 0.75 (0.68–0.81). Agreement for the location of Bruch's membrane opening and the location of retinal pigment epithelium tips was stronger between the automated technique and each individual observer than it was between the two observers.

Conclusions: Larger ßPPA area, as determined by automated OCT assessment, is significantly associated with a diagnosis of glaucoma, even after adjusting for age and axial length, and can aid in differentiating healthy from glaucomatous eyes.

INTRODUCTION

Parapapillary atrophy (PPA) occurs adjacent to the optic disc and represents a complete loss of retinal pigment epithelium (RPE), an almost complete loss of retinal photoreceptors and a partial closure of the choriocapillaris.[1,2] It was formerly called "halo glaucomatosus"[3] due to its association with severe glaucomatous damage.[3–8] PPA occurs more often in glaucomatous than non-glaucomatous eyes and is associated with an increase in the risk of glaucoma progression.[9–14] PPA is also associated with axial myopia,[7,11,15,16] which limits its use for the diagnosis of glaucoma.[17]

In the clinical setting, PPA is typically divided into two subgroups. The alpha PPA zone (αPPA) consists of regions of hypopigmentation and hyperpigmentation of the retinal pigment epithelium and mostly intact photoreceptors, and is usually located peripherally to beta PPA zone ßPPA), when the latter is also present. Histologically, αPPA is equivalent to irregularities of the RPE overlying an intact Bruch's membrane (BM).[1,3,11,16] ßPPA is characterized clinically by visible sclera and large choroidal vessels.[1,3,11,18]

Recent advances in spectral-domain OCT imaging have facilitated the detection of Bruch's membrane opening (BMO) and has led to the identification of different subtypes of beta PPA: Beta-zone ßPPA) and gamma-zone PPA.[11,12] ßPPA is the PPA area with intact BM but without RPE, while gamma-zone PPA is the PPA area without BM and is located between the optic disc clinical border and the edge of BM [1,3,11,16] (Figure 1). Based on manual delineation of the PPA subtypes of OCT images, bot ßPPA and gamma-zone PPA area have been shown to be associated with increased axial length, [19,20] while ßPPA is consistently larger in glaucoma eyes than healthy eyes.[19–21] It has been suggested that ßPPA may be an age-related atrophic change and more strongly associated with glaucoma, while gamma PPA may be due to scleral stretching associated with elongation of the globe in myopia. [14,22,23]

For these reasons, it has been suggested that distinguishing between these 2 PPA subtypes may help to differentiate between myopic eyes with and without glaucoma and/or identify eyes at risk of glaucomatous progression,[11,12,14] There are a limited number of studies evaluating this issue with mixed results. [11,13,19,24,25]

The San Diego Automated Segmentation Algorithm (SALSA) was developed to segment retinal layers from OCT images, [26,27] and now includes the ability to measure the area of ßPPA with intact BM. The purpose of this report is to determine whether the automated measurement of ßPPA area can be used to differentiate between glaucoma and healthy eyes with a wide range of axial lengths (AL).

MATERIALS AND METHODS

Participants

This cross-sectional study included subjects from 2 longitudinal observational cohort studies, the Diagnostic Innovations in Glaucoma Study (DIGS, clinicaltrials.gov identifier NCT00221897); and the African Descent and Glaucoma Evaluation Study (ADAGES, clinicaltrials.gov identifier NCT00221923).[28–30] The Institutional Review Boards of the University of California San Diego, University of Alabama, Birmingham, and of the New York Eye and Ear Infirmary approved the protocol, and the methodology adheres to the tenets of the Declaration of Helsinki.

All subjects were at least 18 years old and required to have open anterior chamber angles upon gonioscopy. Healthy subjects were defined as individuals without clinical signs of retinal or glaucomatous pathologies based on a clinical examination including ophthalmoscopy with medically dilated pupils, and a reliable visual field test without evidence of repeatable visual field damage on Standard Automated Perimetry (SAP). Glaucoma patients were defined as individuals who had glaucomatous optic neuropathy on dilated clinical examination and at least two consecutive, reliable (<33% fixation losses and false negatives, and <15% false positives) and repeatable abnormal SAP tests with the Humphrey 24–2 Swedish Interactive Threshold Algorithm with Pattern Standard Deviation or a Glaucoma Hemifield Test results outside the normal limits. Healthy and glaucoma eyes were selected to be of similar ages and to reflect a wide range of axial lengths.

OCT Image Acquisition

Spectral domain optical coherence tomography (SD-OCT) (Spectralis HRA+OCT; Heidelberg Engineering Inc., Heidelberg, Germany) was used to acquire 48 high-resolution EDI-OCT radial scans centered on the ONH. The scan settings included an automatic real time (ART) mode of 9 frames, 73 sections, a B-scan distance of approximately 7 microns between each A-scan, and 1024 A-scans scans per B-scan. BMO area was measured from Spectralis OCT optic disc scans using the San Diego Automated Layer Segmentation Algorithm (SALSA).[26]

Parapapillary Atrophy Zone Identification

Areas of the ßPPA were automatically identified by calculating the area between the BMO and RPE tips in SD-OCT radial B-scans using SALSA. Details of SALSA and its validation have been described previously.[26,27,31,32,33] Two ophthalmologists (PICM, MHS), masked to patient diagnosis, independently identified the borders of ßPPA by manually marking the 2 RPE tips and the 2 BMO locations on each EDI-OCT radial B-scans of 35 eyes (Fig. 1) using a custom software program in MATLAB.[34] The EDI radial scans consisted of 48 individual radial scans. Every other B-scan was selected for manual delineation resulting in delineation of 24 equidistant scans. ßPPA borders identified manually were then compared to SALSA identification of the location of the BMO and RPE tips.

Statistical Analysis

The associations between the automatically calculated ßPPA area with age, AL, intraocular pressure (IOP), BMO area and central corneal thickness (CCT) in healthy subjects and glaucoma patients was evaluated using STATA. [35] Ordinary least squares regression with the cluster option to adjust for the correlation between eyes within subjects was utilized. Univariate and multivariable linear and logistic regressions were completed to evaluate the association of ßPPA area and diagnosis, respectively after controlling for age and other ocular parameters. Semipartial correlation coefficients (R^2) were calculated to adjust for age in the correlations between ßPPA area and axial length in healthy and glaucoma eyes. The diagnostic accuracy of ßPPA area for differentiating between healthy and glaucoma eyes was assessed by calculating the age- and axial length-adjusted area under the Receiver Operating Characteristic Curve (AUROC), as previously described.[36] Agreement between observers and the automated detection of the location of the BMO and RPE (in pixels) was assessed using Bland-Altman plots and summarized as the 95% confidence interval (CI) limits of agreement of the mean difference in pixels.

RESULTS

Two hundred and twenty-six eyes from 88 glaucoma patients and 38 healthy subjects were included (Table 1). Glaucoma participants had a mean age of 64.2 ± 9.4 years, (median = 66.9 years), a mean visual field (VF) mean deviation (MD) of −5.0 + 6.4 dB (median = −2.6 dB), and mean axial length (AL) of 25.1 + 1.1 mm (median = 25.0 mm). Healthy participants had a mean age of 60.6 + 10.4 years (median = 59.0 years), a mean VF MD of 0.1 + 1.4 dB (median = 0.5 dB), and mean AL of 24.1 + 1.1 mm (median = 24.0 mm). Glaucoma patients had significantly larger ßPPA area ($p<0.001$), longer axial lengths ($p<0.001$), and worse VF MD ($p<0.001$) than healthy eyes.

In univariate analysis of healthy and glaucoma eyes, the automatically delineated ßPPA area increased with longer axial length ($R^2= 30.1\%$; $p<0.001$) (Table 2). The age-adjusted association between ßPPA area and axial length was stronger in glaucoma eyes ($R^2= 24.6\%$ $p<0.001$) than healthy eyes ($R^2= 19.9\%$, $p=0.009$) (Figure 2).

We also evaluated the univariate and multivariable association of age, AL, BMO area, IOP, CCT, and glaucoma diagnosis with ßPPA area as a dependent variable (Table 2). Older age, longer AL, larger BMO area, diagnosis of glaucoma, and higher intraocular pressure (IOP) were each significantly associated with ßPPA area in univariate analysis. In multivariable analysis, larger ßPPA area was significantly associated with a diagnosis of glaucoma and longer AL. This multivariable model explained 36.9% (R^2) of the variance in ßPPA area.

In addition, we completed multivariable logistic regression analysis with glaucoma diagnosis as the dependent variable and controlling for age, axial length, BMO area, IOP, and CCT. We found that the presence of glaucoma was significantly associated with larger ßPPA area. Specifically, for each 0.2 mm^2 higher ßPPA area, the odds of having glaucoma were doubled (odds ratio (95% CI:)) 2.1 (1.2 – 3.6) p = 0.007, Table 3).

The diagnostic accuracy of ßPPA area for differentiating between healthy and glaucoma eyes was also evaluated (Figure 3). The age- and axial length-adjusted AUROC (95% CI) for ßPPA area was 0.75 (0.68–0.81).

Bland-Altman plots were constructed to assess the agreement between the 2 observers and automated assessment of the RPE tips and BMO (Figures 4 and 5). Better agreement was found between automated detection by SALSA and each of the individual graders for both the RPE tip and BMO identification (95% CI for grader 1: approximately 90 and 32 pixels, respectively; and grader 2: approximately 40 and 15 pixels, respectively), than the interobserver agreement between the 2 graders (95% CI approximately 120 pixels and 38 pixels, respectively).

DISCUSSION

Our results suggest that automated calculation of ßPPA area has good agreement with manual expert assessment and has potential for improving our ability to differentiate between healthy and glaucoma eyes. Specifically, larger ßPPA area was significantly associated with a diagnosis of glaucoma, even after adjusting for age and axial length. Moreover, the odds of having glaucoma were doubled for each 0.2 mm^2 larger ßPPA area.

Dai et al.[11] reported that the width and area of the ßPPA was significantly associated with longer axial length and the presence of glaucoma, while the width and area of the gamma zone was significantly associated with myopia, longer axial length, and the absence of glaucoma. Although not investigated in this study, larger ßPPA area has been shown to be associated with an increased risk of progression of VF damage in patients with glaucoma, while gamma zone is more strongly correlated with increased axial length. [19,37]

With an age and axial length adjusted AUROC of 0.75 (Figure 3), our results suggest that ßPPA area may improve our ability to detect glaucoma. These results are in contrast to a report by Vianna et al.[24] that found no significant association between ßPPA area and glaucoma in myopic eyes (AUROC = 0.60). There are several possible explanations for the differences between the current study and the investigation performed by Vianna and colleagues. First, over 90% of their study subjects were of European descent, whereas less than 50% of our subjects were of European descent (Table 1). Second, Vianna et al also limited their study population to myopic eyes with ßPPA, while our study included eyes with a range of axial lengths. As the authors suggest, including eyes that already had increased ßPPA would likely result in a weaker association of beta-PPA and glaucoma than including the general population in the analysis.

Our study demonstrated that ßPPA can be automatically detected from radial EDI ONH B-scans by calculating the area between the BMO and RPE tips. Automatic delineation can facilitate the routine assessment of ßPPA area and width in the nasal area, as well as the temporal area. Manual delineation of the RPE tip and BMO margin in the nasal area is challenging. For this reason, some studies focused on manual assessment of ßPPA width only in the temporal area.[12,37] The agreement between automated detection of both structures and each individual grader was similar or better than the inter-grader agreement of

manual BMO and RPE detection. BMO detection had better inter-grader agreement than RPE tip detection due to the easier identification of BMO compared to RPE in most eyes. [26] BMO identification with SALSA has been shown to have good reproducibility in a previous study (coefficient of variation < 4%). [26] These results are also consistent with other studies suggesting that the detection of the BMO is easier than detection of the RPE tip, due to factors such as disc ovality, blood vessel shadowing and poor image quality that makes detection of RPE challenging.[12,38]

It has been suggested that ßPPA and gamma zone have different underlying pathophysiologies and that the probability of development and progression of glaucoma may differ in eyes with ßPPA and gamma PPA.[12] Myopia-related PPA versus PPA related to aging or glaucoma may also have different underlying mechanisms.[39] While it is unclear which factors lead to an increased susceptibility of myopic eyes to glaucoma,[40–46] individuals with high myopia are 2.5 times more likely to have glaucoma, based on a meta-analysis of 7 studies (odds ratios (95% CI): 2.46 (1.93 to 3.15). [44] Other studies have been suggested that glaucoma may be over-diagnosed and overtreated in individuals with high myopia.[47–52] While recent advances in technology have contributed to faster and more efficient ways of diagnosing eye disease, [53] diagnosis of glaucoma in eyes with myopia has remained challenging. Automatic differentiation of the ßPPA zone in its new OCT-based definition may facilitate better detection of glaucoma in myopic eyes, as myopic optic nerve heads present significant challenges to diagnosing this disease correctly,[49] and facilitation of identifying eyes at risk of progression. [25]

There are several limitations to our study. First, the sample size, although similar to previously published studies on ßPPA area,[11,12,24,54] was relatively small. Second, as in other reports, our glaucoma group was older than the normal controls,[11,24,37] though the difference did not reach statistical significance. For this reason, age was included in the multivariable analysis and the values of age-adjusted area under the receiver operating characteristic curve are reported. Future studies should include a larger sample of age-matched patients with higher myopia or longer AL, in order to better evaluate ßPPA in patients with longer axial lengths in both healthy and glaucoma groups, as well as the impact of AL on the diagnostic accuracy of ßPPA. Third, we did not include automated analysis of gamma PPA area. While SALSA was able to detect ßPPA in all eyes that were manually segmented, automated detection of gamma PPA detection was found to be more challenging as the detection of the optic disc margin, defined as the border of the lamina cribrosa or as the intraocular projection of the optic nerve pia mater, is more difficult. We are currently working on methods to automate the detection of gamma PPA area.

In conclusion, larger ßPPA area was associated with an increased risk of having glaucoma in eyes with a range of axial lengths. Automated calculation of ßPPA area shows promise for aiding in the differentiation of eyes with glaucoma from those without glaucoma. Further studies are needed to determine the usefulness of automated calculation of ßPPA area for detecting glaucoma in the growing population of high myopes

ACKNOWLEDGEMENTS

a. A Funding/Support: This study was supported by the following NIH grants: Vision Research Core Grant P30EY022589, EY11008, EY019869, EY021818, EY027510 and an unrestricted grant from Research to Prevent Blindness (New York, NY). Participant retention incentive grants were given in the form of glaucoma medications from Alcon Laboratories, Inc., Allergan, Pfizer Inc., and Santen Inc. at no cost.

b. Financial Disclosures: Patricia Isabel C. Manalastas, Akram Belghith, Min Hee Suh, and Adeleh Yarmohammadi have nothing to disclose.

Jost B. Jonas: *patent holder with Biocompatibles UK Ltd. (Franham, Surrey, UK) (Title: Treatment of eye diseases using encapsulated cells encoding and secreting neuroprotective factor and/ or anti-angiogenic factor; Patent number: 20120263794), and patent application with University of Heidelberg (Heidelberg, Germany) (Title: Agents for use in the therapeutic or prophylactic treatment of myopia or hyperopia; Europäische Patentanmeldung 15 000 771.4).*

Robert N. Weinreb: Aerie Pharmaceuticals, *Alcon, Allergan, Bausch+Lomb, Eyenovia, Unity, Valeant (C); Heidelberg Engineering, Carl Zeiss Meditec, Genentech, Konan, National Eye Institute, Neurovision, OptoVue, Quark, Reichert, Tomey, Topcon (F); Carl Zeiss Meditec (R)*

Felipe A. Medeiros: *Carl-Zeiss Meditec, Heidelberg Engineering, Topcon, Ametek, Bausch+Lomb, Allergan, Sensimed (F); Carl-Zeiss Meditec, Heidelberg Engineering, Ametek, Alcon, Allergan (C); Carl Zeiss Meditec Inc. (R)*

Christopher A. Girkin: Consultant - Alcon Laboratories Inc., Allergan Inc., Pfizer Inc.; Research support - Heidelberg Engineering GmbH, Optovue Inc., Merck Inc., Topcon Medical Systems, Inc., Carl Zeiss Meditec, Inc.

Jeffrey M. Liebmann: Consultant - Aerie Pharmaceuticals, Inc., Alcon Laboratories Inc., Allergan Inc., Bausch & Lomb, Inc., Carl Zeiss Meditec Inc., Dyopsis Inc., ForSight Vision5, Inc., Inotek Pharmaceuticals, Inc., Topcon Medical Systems, Inc.

Linda M. Zangwill: *Carl Zeiss Meditec Inc., Heidelberg Engineering GmbH, Optovue Inc., Topcon Medical Systems Inc. (F); Carl Zeiss Meditec Inc., Optovue Inc. (R)*

c. Other Acknowledgements: None.

REFERENCES

1. Jonas JB, Nguyen XN, Gusek GC, Naumann GO. Parapapillary chorioretinal atrophy in normal and glaucoma eyes. I. Morphometric data. Invest Ophthalmol Vis Sci. 5 1989;30(5):908–918. [PubMed: 2722447]
2. Fantes FE, Anderson DR. Clinical histologic correlation of human peripapillary anatomy. Ophthalmology. 1 1989;96(1):20–25. [PubMed: 2919048]
3. Jonas JB, Fernandez MC, Naumann GO. Glaucomatous parapapillary atrophy. Occurrence and correlations. Arch Ophthalmol. 2 1992;110(2):214–222. [PubMed: 1736871]
4. Jonas JB, Hayreh SS, Tao Y. Clinicopathological correlation of parapapillary atrophy in monkeys with experimental glaucoma and temporary central retinal artery occlusion. Indian J Ophthalmol. 2 2014;62(2):219–223. [PubMed: 23619503]
5. Xu L, Wang Y, Yang H, Jonas JB. Differences in parapapillary atrophy between glaucomatous and normal eyes: the Beijing Eye Study. Am J Ophthalmol. 10 2007;144(4):541–546. [PubMed: 17651676]
6. Budde WM, Jonas JB. Enlargement of parapapillary atrophy in follow-up of chronic open-angle glaucoma. Am J Ophthalmol. 4 2004;137(4):646–654. [PubMed: 15059703]
7. Guo Y, Wang YX, Xu L, Jonas JB. Five-year follow-up of parapapillary atrophy: the Beijing Eye Study. PLoS One. 2012;7(5):e32005. [PubMed: 22586440]
8. Jonas JB, Budde WM, Lang PJ. Parapapillary atrophy in the chronic open-angle glaucomas. Graefes Arch Clin Exp Ophthalmol. 10 1999;237(10):793–799. [PubMed: 10502052]
9. Uchida H, Ugurlu S, Caprioli J. Increasing peripapillary atrophy is associated with progressive glaucoma. Ophthalmology. 8 1998;105(8):1541–1545. [PubMed: 9709771]

10. Heltzer JM. Progression of peripapillary atrophy. Ophthalmology. 51999;106(5):857.
11. Dai Y, Jonas JB, Huang H, Wang M, Sun X. Microstructure of parapapillary atrophy: beta zone and gamma zone. Invest Ophthalmol Vis Sci. 3 2013;54(3):2013–2018. [PubMed: 23462744]
12. Kim M, Kim TW, Weinreb RN, Lee EJ. Differentiation of parapapillary atrophy using spectral-domain optical coherence tomography. Ophthalmology. 9 2013;120(9):1790–1797. [PubMed: 23672970]
13. Teng CC, De Moraes CG, Prata TS, Tello C, Ritch R, Liebmann JM. Beta-Zone parapapillary atrophy and the velocity of glaucoma progression. Ophthalmology. 5 2010;117(5):909–915. [PubMed: 20132988]
14. Lee EJ, Kim TW, Weinreb RN, Park KH, Kim SH, Kim DM. beta-Zone parapapillary atrophy and the rate of retinal nerve fiber layer thinning in glaucoma. Invest Ophthalmol Vis Sci. 6 2011;52(7): 4422–4427. [PubMed: 21474770]
15. Xu L, Wang YX, Wang S, Jonas JB. Definition of high myopia by parapapillary atrophy. The Beijing Eye Study. Acta Ophthalmol. 12 2010;88(8):e350–351. [PubMed: 19900199]
16. Dai Y, Jonas JB, Ling Z, Sun X. Ophthalmoscopic-Perspectively Distorted Optic Disc Diameters and Real Disc Diameters. Invest Ophthalmol Vis Sci. 11 2015;56(12):7076–7083. [PubMed: 26536062]
17. Law SK, Lin SC, Singh K. Clinical Update Glaucoma: Myopia and Glaucoma: Sorting Out the Diagnosis. Eyenet; 2013:35–37.
18. Jonas JB. Clinical implications of peripapillary atrophy in glaucoma. Curr Opin Ophthalmol. 4 2005;16(2):84–88 [PubMed: 15744137]
19. Jonas JB, Jonas SB, Jonas RA, et al. Parapapillary atrophy: histological gamma zone and delta zone. PLoS One. 2012;7(10):e47237. [PubMed: 23094040]
20. Miki A, Ikuno Y, Weinreb RN, et al. Measurements of the parapapillary atrophy zones in en face optical coherence tomography images. PLoS One. 2017;12(4):e0175347. [PubMed: 28414805]
21. Akagi T, Hangai M, Kimura Y, et al. Peripapillary scleral deformation and retinal nerve fiber damage in high myopia assessed with swept-source optical coherence tomography. Am J Ophthalmol. 5 2013;155(5):927–936. [PubMed: 23434206]
22. Park SC, De Moraes CG, Tello C, Liebmann JM, Ritch R. In-vivo microstructural anatomy of beta-zone parapapillary atrophy in glaucoma. Invest Ophthalmol Vis Sci. 12 2010;51(12):6408–6413. [PubMed: 20631234]
23. Chrastek R, Wolf M, Donath K, et al. Automated segmentation of the optic nerve head for diagnosis of glaucoma. Med Image Anal. 8 2005;9(4):297–314. [PubMed: 15950894]
24. Vianna JR, Malik R, Danthurebandara VM, et al. Beta and Gamma Peripapillary Atrophy in Myopic Eyes With and Without Glaucoma. Invest Ophthalmol Vis Sci. 6 1 2016;57(7):3103–3111. [PubMed: 27294804]
25. Kim YW, Lee EJ, Kim TW, Kim M, Kim H. Microstructure of beta-zone parapapillary atrophy and rate of retinal nerve fiber layer thinning in primary open-angle glaucoma. Ophthalmology. 7 2014;121(7):1341–1349. [PubMed: 24565742]
26. Belghith A, Bowd C, Medeiros FA, et al. Does the Location of Bruch's Membrane Opening Change Over Time? Longitudinal Analysis Using San Diego Automated Layer Segmentation Algorithm (SALSA). Invest Ophthalmol Vis Sci. 2 1 2016;57(2):675–682. [PubMed: 26906156]
27. Belghith A, Bowd C, Weinreb RN, Zangwill LM. A hierarchical framework for estimating neuroretinal rim area using 3D spectral domain optical coherence tomography (SD-OCT) optic nerve head (ONH) images of healthy and glaucoma eyes. Conf Proc IEEE Eng Med Biol Soc. 2014;2014:3869–3872. [PubMed: 25570836]
28. Sample PA, Girkin CA, Zangwill LM, et al. The African Descent and Glaucoma Evaluation Study (ADAGES): design and baseline data. Arch Ophthalmol. 9 2009;127(9):1136–1145. [PubMed: 19752422]
29. Medeiros FA, Zangwill LM, Bowd C, Weinreb RN. Comparison of the GDx VCC scanning laser polarimeter, HRT II confocal scanning laser ophthalmoscope, and stratus OCT optical coherence tomograph for the detection of glaucoma. Arch Ophthalmol. 6 2004;122(6):827–837. [PubMed: 15197057]

30. Sample PA, Medeiros FA, Racette L, et al. Identifying glaucomatous vision loss with visual-function-specific perimetry in the diagnostic innovations in glaucoma study. Invest Ophthalmol Vis Sci. 8 2006;47(8):3381–3389. [PubMed: 16877406]
31. Belghith A et al. 2015. Automated segmentation of anterior lamina cribrosa surface: How the lamina cribrosa responds to intraocular pressure change in glaucoma eyes? Conf Proc IEEE Eng Med Biol Soc 2015: p. 222–225 [PubMed: 26736240]
32. Mundae RS, Zangwill LM, Kabbara SW, et al. A Longitudinal Analysis of Peripapillary Choroidal Thinning in Healthy and Glaucoma Subjects. Am J Ophthalmol. 2 2018;186:89–95. [PubMed: 29103960]
33. Kabbara SW, Zangwill LM, Mundae R, et al. Comparing optical coherence tomography radial and cube scan patterns for measuring Bruch's membrane opening minimum rim width (BMO-MRW) in glaucoma and healthy eyes: crosssectional and longitudinal analysis. Br J Ophthalmol. 3 2018;102(3):344–351. [PubMed: 28774935]
34. MATLAB version 8.5. Natick, Massachusetts: The MathWorks Inc., 2015.
35. StataCorp. 2015 Stata Statistical Software: Release 14. College Station, TX: StataCorp LP.
36. Medeiros FA, Sample PA, Zangwill LM, Liebmann JM, Girkin CA, Weinreb RN. A statistical approach to the evaluation of covariate effects on the receiver operating characteristic curves of diagnostic tests in glaucoma. Invest Ophthalmol Vis Sci. 6 2006;47(6):2520–2527. [PubMed: 16723465]
37. Yamada H, Akagi T, Nakanishi H, et al. Microstructure of Peripapillary Atrophy and Subsequent Visual Field Progression in Treated Primary Open-Angle Glaucoma. Ophthalmology 3 2016;123(3):542–551. [PubMed: 26692299]
38. Kimura Y, Akagi T, Hangai M, et al. Lamina cribrosa defects and optic disc morphology in primary open angle glaucoma with high myopia. PLoS One. 2014;9(12):e115313. [PubMed: 25531656]
39. Hwang YH, Jung JJ, Park YM, Kim YY, Woo S, Lee JH. Effect of myopia and age on optic disc margin anatomy within the parapapillary atrophy area. Jpn J Ophthalmol. 9 2013;57(5):463–470. [PubMed: 23851575]
40. Czudowska MA, Ramdas WD, Wolfs RC, et al. Incidence of glaucomatous visual field loss: a ten-year follow-up from the Rotterdam Study. Ophthalmology. 9 2010;117(9):1705–1712. [PubMed: 20591487]
41. Mitchell P, Hourihan F, Sandbach J, Wang JJ. The relationship between glaucoma and myopia: the Blue Mountains Eye Study. Ophthalmology. 10 1999;106(10):2010–2015. [PubMed: 10519600]
42. Ramakrishnan R, Nirmalan PK, Krishnadas R, et al. Glaucoma in a rural population of southern India: the Aravind comprehensive eye survey. Ophthalmology. 8 2003;110(8):1484–1490. [PubMed: 12917161]
43. Xu L, Wang Y, Wang S, Wang Y, Jonas JB. High myopia and glaucoma susceptibility the Beijing Eye Study. Ophthalmology. 2 2007;114(2):216–220. [PubMed: 17123613]
44. Marcus MW, de Vries MM, Junoy Montolio FG, Jansonius NM. Myopia as a risk factor for open-angle glaucoma: a systematic review and meta-analysis. Ophthalmology. 10 2011;118(10):1989–1994 e1982. [PubMed: 21684603]
45. Khachatryan N, Medeiros FA, Sharpsten L, et al. The African Descent and Glaucoma Evaluation Study (ADAGES): predictors of visual field damage in glaucoma suspects. American journal of ophthalmology. 4 2015;159(4):777–787. [PubMed: 25597839]
46. Nagaoka N, Jonas JB, Morohoshi K, et al. Glaucomatous-Type Optic Discs in High Myopia. PLoS One. 2015;10(10):e0138825. [PubMed: 26425846]
47. Kim KE, Jeoung JW, Park KH, Kim DM, Kim SH. Diagnostic Classification of Macular Ganglion Cell and Retinal Nerve Fiber Layer Analysis. Ophthalmology. 2015;122(3):502–510. [PubMed: 25444638]
48. Doshi A, Kreidl KO, Lombardi L, Sakamoto DK, Singh K. Nonprogressive glaucomatous cupping and visual field abnormalities in young Chinese males. Ophthalmology. 3 2007;114(3):472–479. [PubMed: 17123617]
49. Chang RT, Singh K. Myopia and glaucoma: diagnostic and therapeutic challenges. Curr Opin Ophthalmol. 3 2013;24(2):96–101. [PubMed: 23542349]

50. Lee JY, Sung KR, Han S, Na JH. Effect of myopia on the progression of primary open angle glaucoma. Investigative ophthalmology & visual science. 2 19, 2015 2015.

51. Hsu CH, Chen RI, Lin SC. Myopia and glaucoma: sorting out the difference. Curr Opin Ophthalmol. 3 2015;26(2):90–95. [PubMed: 25565367]

52. Jonas JB, Xu L. Histological changes of high axial myopia. Eye. 2 2014;28(2):113–117. [PubMed: 24113300]

53. Greenfield DS, Weinreb RN. Role of optic nerve imaging in glaucoma clinical practice and clinical trials. Am J Ophthalmol. 4 2008;145(4):598–603. [PubMed: 18295183]

54. Hayashi K, Tomidokoro A, Lee KY, et al. Spectral-domain optical coherence tomography of beta-zone peripapillary atrophy: influence of myopia and glaucoma. Invest Ophthalmol Vis Sci. 3 2012;53(3):1499–1505. [PubMed: 22323471]

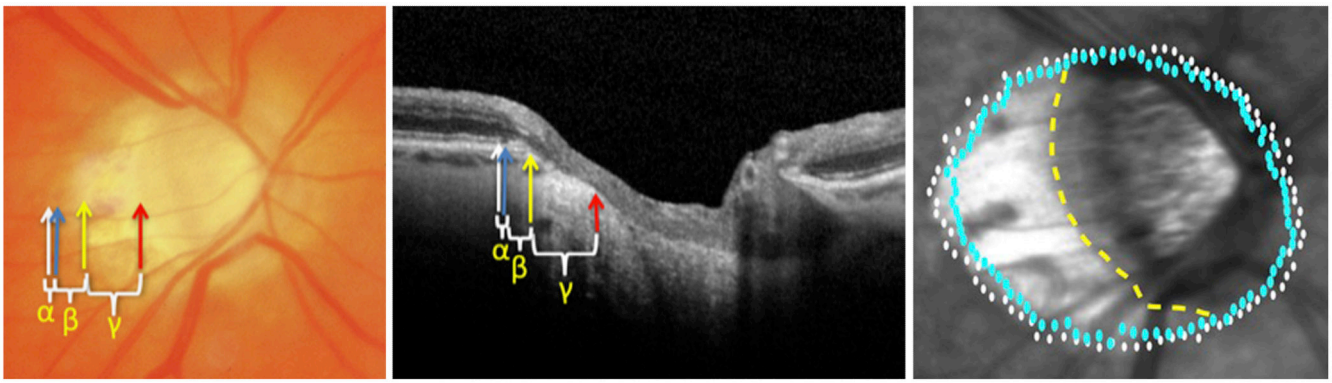

Figure 1:
Example of manual delineation and automated identification of retinal pigment epithelial (RPE) tips and Bruch's Membrane (BM). Left: Manual delineation on an optic nerve head photograph and on an individual B-scan (middle). Alpha (α) parapapillary atrophy (PPA) is located between the white and blue arrows (RPE tip). Beta (β) PPA is located between blue (RPE tip) and yellow (BM) arrows. Gamma (γ) PPA is located between the yellow and red arrows. Right: Automated delineation of βPPA area is located between the BM (blue dots) and RPE tips (white dots). Clinical βPPA (manual dashed yellow line to white dots) cannot distinguish between βPPA & gamma PPA, as the BM is only visible with OCT.

Figure 2:
Linear regression for the relationship between beta zone area and axial length for healthy and glaucoma eyes, showing that a larger automatically calculated βPPA zone area was more strongly associated with axial length in glaucoma eyes (R^2 = 24.6%), than in healthy eyes (R^2 = 19.9%) after adjust for age.

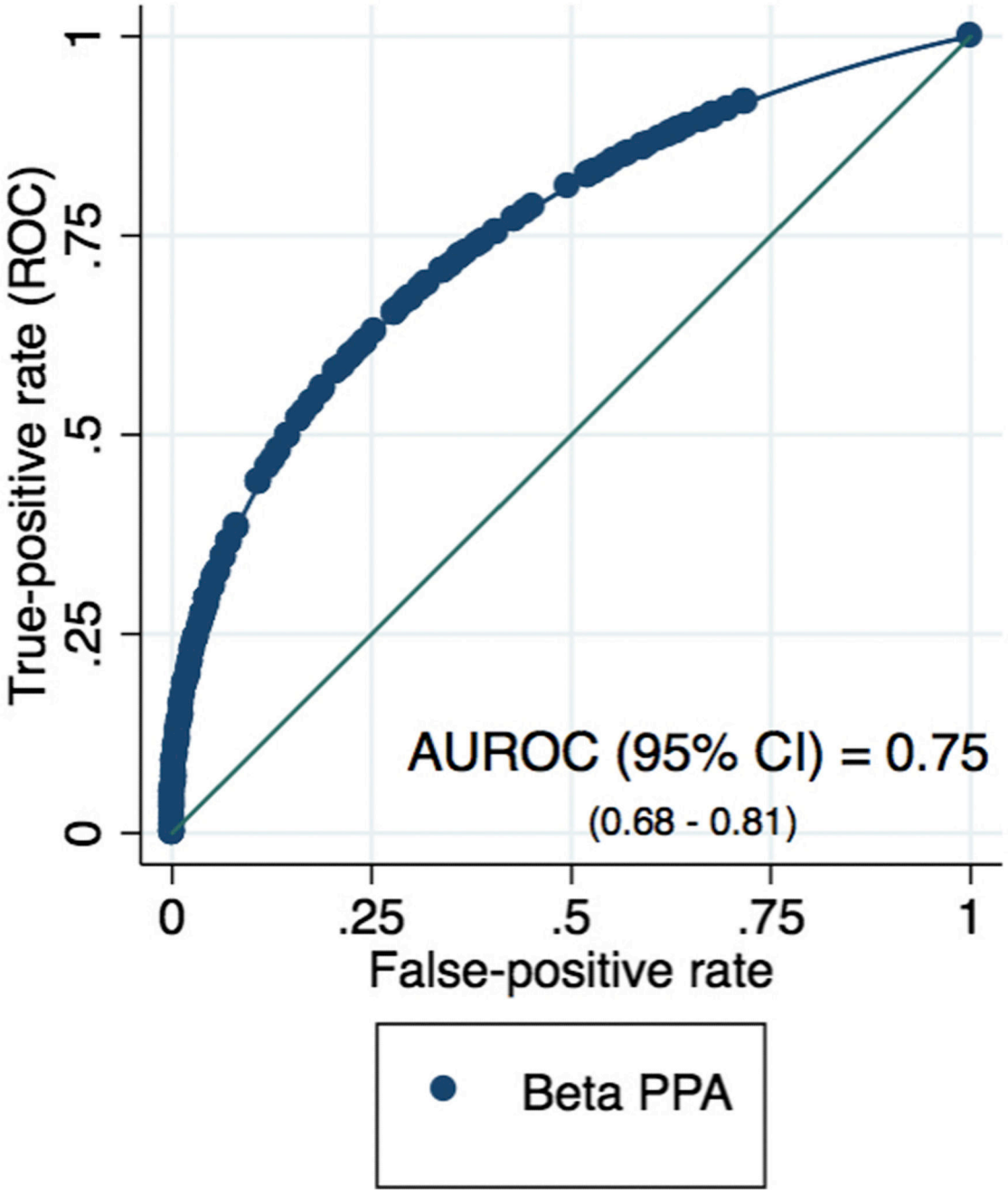

Figure 3:
The receiver operating characteristic curve of ßPPA area for differentiating between healthy and glaucoma eyes. The age- and axial length-adjusted area under the receiver operating characteristic curve (AUROC) (95% CI) is 0.75 (0.68–0.81).

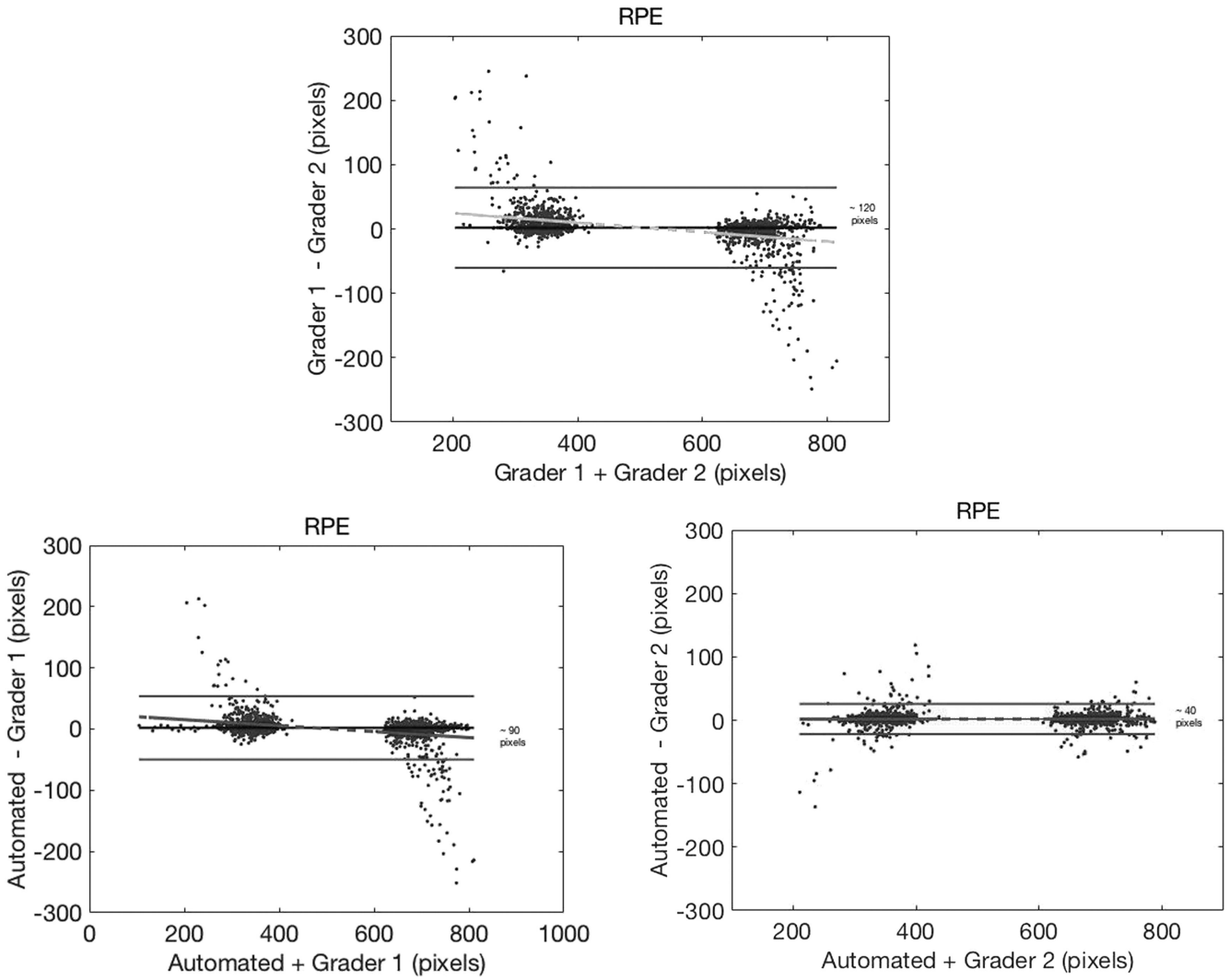

Figure 4:

Bland-Altman plots for retinal pigment epithelium (RPE) tip identification, with 95% confidence interval (CI) (top) inter-grader agreement of ~120 pixels, (lower left) automated RPE detection versus grader 1 agreement of ~90 pixels, and (lower right) automated RPE detection versus grader 2 agreement of ~40 pixels. Please note that every B-scan has 2 RPE tip locations.

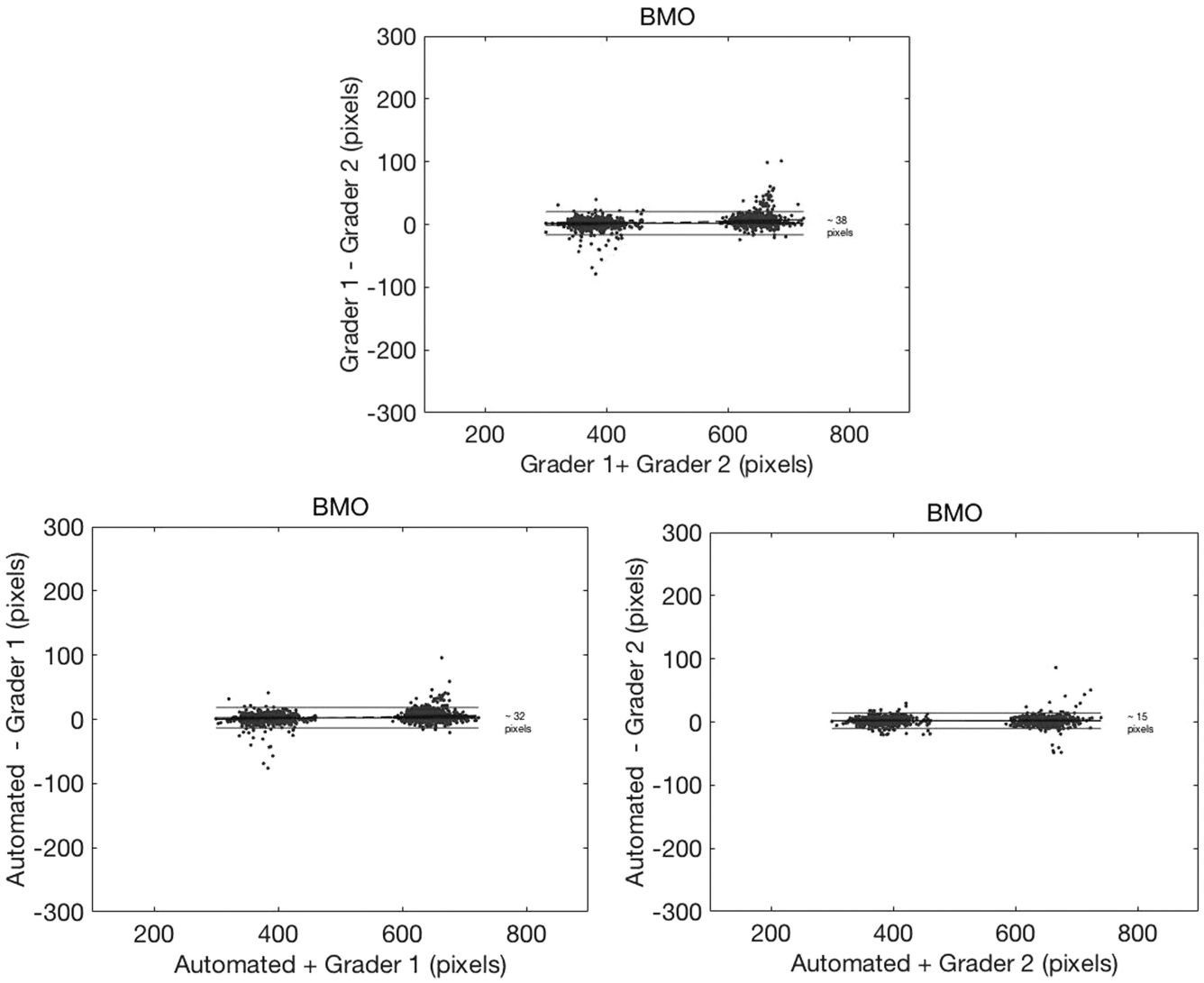

Figure 5:

Bland-Altman plots for Bruch's membrane opening (BMO) identification, with 95% confidence interval (CI) (top) inter-grader agreement of ~38 pixels, (lower left) automated BMO detection versus grader 1 agreement of ~32 pixels, and (lower right) automated BMO detection versus grader 2 agreement of ~15 pixels. Please note that every B-scan has 2 BMO locations.

Table 1:

Patient Demographics [a]

Variable	*Healthy (N=73 eyes; 38 subjects)*	*Glaucoma (N=153 eyes; 88 subjects)*	*p value*
Age (years)	60.6 (57.2 – 64.1)	64.2 (62.2 – 66.2)	0.060 *
Gender: n (%)			0.052 *
Male	14 (36.8%)	49 (55.7%)	
Female	24 (63.2%)	39 (44.3%)	
Race: n (%)			0.775 *
European Descent	19 (50.0%)	46 (38.6%)	
African Descent	14 (36.8%)	34 (52.3%)	
Other	5 (13.2%)	8 (9.1%)	
Axial length (mm)	24.1 (23.8 – 24.4)	25.1 (24.9 – 25.3)	<0.001
CCT [b] (um)	555.4 (546.4 – 564.4)	548.1 (541.4 – 554.8)	0.208
BMO area (mm^2)	2.05 (1.94 – 2.16)	2.26 (2.18 – 2.34)	0.003
VF MD [c] (dB)	0.19 (−0.13 – 0.51)	−5.08 (−6.11 – −4.05)	<0.001
ßPPA area [d] (mm^2)	0.72 (0.68 – 0.77)	0.91 (0.88 – 0.94)	<0.001
Refraction (D)	−0.99 (−1.43 – −0.56)	−2.43 (−2.80 – −2.05)	<0.001
IOP [e] (mmHg)	14.1 (13.5 – 14.8)	14.0 (13.4 – 14.6)	0.819

[a] Values represent means and 95% Confidence intervals unless stated otherwise;

[b] CCT = Central corneal thickness;

[c] VF MD = Visual field mean deviation;

[d] ßPPA = beta parapapillary atrophy;

[e] IOP = Intraocular pressure.

* Statistical analysis by subject

Table 2:

Association ßPPA surface area with age, ocular parameters and glaucoma diagnosis: Univariate and Multivariable Analysis (n = 226)

	Univariate			Multivariable		
Variable	Coefficient (95% Confidence Interval)	p value	R^2	Coefficient (95% Confidence Interval)	p Value	R^2
Age	0.003 (0.000 – 0.006)	**0.043**	2.2	0.000 (−0.002 – 0.002)	0.879	36.9
AL	0.093 (0.072 – 0.115)	**<0.001**	30.1	0.079 (0.057 – 0.100)	**<0.001**	
CCT	−0.000 (−0.000 – 0.000)	0.838	0.0	0.000 (−0.000 – 0.000)	0.328	
BMO Area	0.065 (0.003 – 0.126)	**0.038**	2.4	0.048 (0.000 – 0.097)	0.052	
IOP	−0.006 (−0.015 – 0.002)	0.841	1.0	−0.003 (−0.008 – 0.002)	0.246	
Diagnosis (1=glaucoma 0=healthy)	0.187 (0.127 – 0.248)	**<0.001**	17.0	0.100 (0.041 – 0.158)	0.001	

ßPPA = beta parapapillary atrophy; AL = Axial length; CCT = Central corneal thickness; IOP = Intraocular pressure.

Table 3:

Multivariable Logistic Regression for Diagnosis of Glaucoma

Variable	Odds Ratio (95% Conf. Interval)	p value	R^2
Age (per 1 year)	1.032 (0.983 – 1.082)	0.197	**21.1%**
AL (per 1 mm)	1.532 (0.877 – 2.675)	0.134	
CCT (per 1 μm)	0.997 (0.986 – 1.008)	0.607	
BMO Area (per 0.4 mm^2)	1.428 (0.936 – 2.179)	0.098	
IOP (per 1 mmHg)	1.054 (0.940 – 1.182)	0.362	
ßPPA (per 0.2 mm^2)	2.086 (1.219 – 3.569)	**0.007**	

AL = Axial length; CCT = Central corneal thickness; IOP = Intraocular pressure; **ß**PPA = beta parapapillary atrophy area.